JOURNAL OF AIRCRAFT
Vol. 44, No. 6, November–December 2007

Optimum Aeorelastic Design of a Flapping Wing

Koji Isogai* and Yohei Harino†
Nippon Bunri University, Oita 870-0397, Japan

DOI: 10.2514/1.27142

A method is presented for the optimum aeroelastic design of a flapping wing employing a lifting-surface theory as an aerodynamic tool and the complex method as the optimization algorithm. The method is applied to the optimum design of a flapping wing of a Kite Hawk (*Milvus migrans*) unmanned air vehicle and the optimum thickness distribution of the main spar is determined. As a result of the optimization, a high propulsive efficiency of 75% is attained considering only dihedral flapping of the main spar. By evaluating the viscous effect for this optimum design using a three-dimensional Navier–Stokes code, the effectiveness of the design is confirmed.

Nomenclature

A	=	X coordinate of pitch axis
a	=	x coordinate of pitch axis
b_0	=	root semichord
b_θ	=	rate of twist of feathering oscillation amplitude
C_{df}	=	viscous drag coefficient
C_L	=	lift coefficient
C_{PW}	=	necessary power coefficient
C_T	=	thrust coefficient ($C_T = C_{TL} + C_{TD}$)
C_{TD}	=	thrust coefficient due to tilt of normal force vector
C_{TL}	=	thrust coefficient due to leading-edge suction
EI	=	bending stiffness parameter at elastic axis
F	=	displacement of wing mean surface
F_r	=	displacement of rigid wing
GJ	=	torsion stiffness parameter about elastic axis
H	=	amplitude of heaving oscillation
K	=	kinetic energy
k	=	reduced frequency defined by $k = b_0\omega/U$
M_i	=	generalized mass
m	=	wing mass per unit area
Q_i	=	generalized force
q_i	=	generalized coordinate
S	=	full span wing area
s	=	semispan divided by b_0
T	=	time
t	=	dimensionless time defined by $t = T(U/b_0)$
U	=	flight velocity
u, v, w	=	dimensionless velocities in x, y, and z directions, respectively
W	=	work
X, Y, Z	=	Cartesian coordinates
x, y, z	=	Cartesian coordinates divided by b_0
α_m	=	mean angle of attack
ΔC_{Pj}	=	pressure difference coefficient due to jth normal mode
$\Delta C_p^{(F)}$	=	pressure difference coefficient due to rigid wing displacement
ΔP	=	pressure difference
η_p	=	propulsive efficiency
$\bar{\theta}$	=	feathering parameter defined by $[\bar{\theta} = \theta_r U/(H_r\omega)]$
θ_0	=	amplitude of feathering oscillation
ξ, η, ζ	=	dimensionless Cartesian coordinates
ρ	=	air density
ϕ	=	phase advance angle of feathering oscillation ahead of flapping oscillation
ϕ_0	=	amplitude of flapping oscillation
ω	=	circular frequency of forced oscillation
ω_i	=	natural circular frequency of oscillation
ω_y	=	vorticity defined by $(\partial w/\partial x - \partial u/\partial z)/2$

Subscripts

e	=	aeroelastic effect
r	=	root station

Superscripts

F	=	rigid wing
$\overline{\ }$	=	time averaged

I. Introduction

BIRDLIKE aerial vehicles with flapping wings have attracted considerable interest for their possible use in wide-ranging monitoring and surveillance activities. Although several such vehicles have been developed to date, most have employed membrane-type wings. However, membrane wings are not efficient because the feathering (twisting) motion, which is essential for efficient flapping flight, does not occur in an ideal manner (a 90 deg advance phase angle of the feathering motion ahead of the flapping motion is usually the most efficient). However, DeLaurier and Harris [1,2] have developed an ornithopter that has double solid surface airfoil sections and uses aeroelastic deformation to generate a twisting motion by dihedral flapping. To obtain favorable aeroelastic deformation, they developed a design program called ComboWing that determines the optimum aeroelastic design of a flapping wing. They employed a strip theory as an aerodynamic tool and conducted the optimization manually, without using an automated optimization algorithm.

The purpose of the present study is to develop an automated optimum aeroelastic design method using a more accurate aerodynamic tool, namely, unsteady lifting-surface theory. The new method is then applied to the design of the flapping wing of a Kite Hawk (*Milvus migrans*) unmanned air vehicle (UAV). The optimum design thus obtained is examined by numerical simulation using a three-dimensional Navier–Stokes (NS) code.

II. Equations of Motion for Elastic Flapping Wing and Solution Procedure Using the Doublet Lattice Method

In this section, the basic equations of motion for an elastic flapping wing are derived using Lagrange's equations of motion. The solution procedure using the doublet lattice method (DLM) [3] as the aerodynamic tool is also described. In Fig. 1, the coordinates and the

Received 7 August 2006; revision received 14 March 2007; accepted for publication 19 June 2007. Copyright © 2007 by the American Institute of Aeronautics and Astronautics, Inc. All rights reserved. Copies of this paper may be made for personal or internal use, on condition that the copier pay the $10.00 per-copy fee to the Copyright Clearance Center, Inc., 222 Rosewood Drive, Danvers, MA 01923; include the code 0021-8669/07 $10.00 in correspondence with the CCC.

*Professor, Micro Flying Robot Laboratory, 1722 Ohaza Ichigi; isogai@nbu.ac.jp. Associate Fellow AIAA.

†Graduate Student, Micro Flying Robot Laboratory, 1722 Ohaza Ichigi.

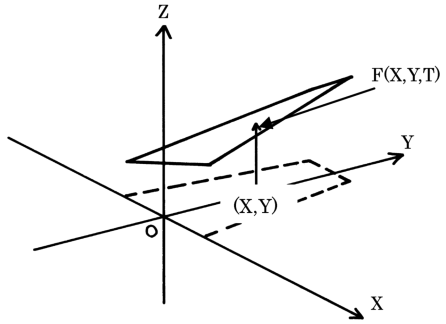

Fig. 1 Definitions of coordinates.

definition of the wing displacement are shown. In the figure, T is time and $F(X, Y, T)$ is the displacement of the wing mean surface at an arbitrary point (X, Y) on the wing. F can be expressed by the following equation:

$$F(X, Y, T) = F_r(X, Y, T) + \sum_{i=1}^{N} \phi_i(X, Y) q_i(T) \tag{1}$$

where $F_r(X, Y, T)$ is the displacement of the rigid wing due to forced oscillation, $\phi_i(X, Y)$ is the ith natural vibration mode of the wing, and $q_i(T)$ is the ith generalized coordinate of the elastic deformation. For this wing displacement, the kinetic energy of the wing can be expressed as

$$K = \iint_S \frac{1}{2} m(X, Y)(\mathrm{d}F/\mathrm{d}T)\, \mathrm{d}X\, \mathrm{d}Y \tag{2}$$

where $m(X, Y)$ is the wing mass per unit area and where $\iint_S$ represents the surface integral on the full span wing area. The strain energy of the wing can be expressed as

$$U = \tfrac{1}{2}\omega_i^2 M_i q_i^2(T) \tag{3}$$

where ω_i is the ith natural circular frequency of the wing, and where M_i is the generalized mass given by

$$M_i = \iint_S m(X, Y)\phi_i^2(X, Y)\, \mathrm{d}X\, \mathrm{d}Y \tag{4}$$

The virtual work done by the external force (aerodynamic force) due to the virtual displacement δq_i of the ith generalized coordinate can be given by

$$\delta W = \iint_S \Delta P(X, Y, T)\phi_i(X, Y)\, \mathrm{d}X\, \mathrm{d}Y \delta q_i \tag{5}$$

where ΔP is the pressure difference between the upper and the lower surfaces of the wing. From Eq. (5) and by the definition of the generalized force Q_i, that is $\delta W = Q_i \delta q_i$, Q_i can be given by

$$Q_i = \iint_S \Delta P(X, Y, T)\phi_i(X, Y)\, \mathrm{d}X\, \mathrm{d}Y \tag{6}$$

Substituting Eqs. (2), (3), and (6) into Lagrange's equations of motion, we finally obtain the general expressions for the equation of motion of an elastic flapping wing as

$$\begin{aligned} M_i(\mathrm{d}^2 q_i/\mathrm{d}T^2) + \omega_i^2 M_i q_i \\ = -\iint_S m(X, Y)\phi_i(X, Y)(\mathrm{d}^2 F_r(X, Y, T)/\mathrm{d}T^2)\, \mathrm{d}X\, \mathrm{d}Y \\ + \iint_S \Delta P(X, Y, T)\phi_i(X, Y)\, \mathrm{d}X\, \mathrm{d}Y, \qquad i = 1, \ldots, N \end{aligned} \tag{7}$$

In deriving Eq. (7), we use the orthogonal condition of the natural vibration modes. In Eq. (7), the displacement $F_r(X, Y, T)$ of the rigid wing or the forced oscillation of the undeformed wing can be expressed as

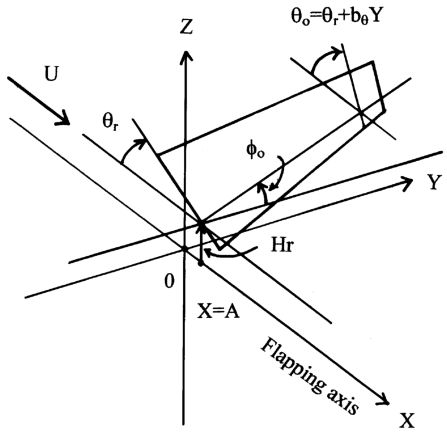

Fig. 2 Definitions of wing motion.

$$\begin{aligned} F_r(X, Y, T) = (H_r + \phi_0 Y)\cos(\omega T) \\ - (\theta_r + b_\theta Y)(X - A)\cos(\omega T + \phi) \end{aligned} \tag{8}$$

where H_r and θ_r are the amplitudes of the heaving and pitching oscillations at the root station, respectively, ϕ_0 is the flapping oscillation amplitude, b_θ is the rate of twist of the feathering oscillation amplitude, A is the X coordinate of the feathering axis, and ϕ is the advance phase angle of the feathering oscillation ahead of the flapping oscillation. (See also Fig. 2 for the definitions of flapping wing motion.)

The load distribution $\Delta P(X, Y, T)$ is expressed as

$$\Delta P(X, Y, T) = \frac{1}{2}\rho U^2 \left\{ \Delta C_P^{(F)}(X, Y, T) + \sum_{j=1}^{N} \Delta \overline{C_{Pj}}(X, Y) q_j(T) \right\} \tag{9}$$

where $\Delta C_P^{(F)}$ is the pressure difference coefficient due to the rigid wing displacement, and $\overline{\Delta C_{Pj}}$ is the pressure difference coefficient due to the jth natural vibration mode. By assuming sinusoidal wing motion and introducing a complex expression, $\Delta C_P^{(F)}$ and q_j can be expressed as

$$\begin{aligned} \Delta C_P^{(F)}(X, Y, T) &= \overline{\Delta C_P^{(F)}}(X, Y) e^{i\omega T} = \overline{\Delta C_P^{(F)}} e^{ikt} \\ q_i &= \overline{q_i} e^{i\omega T} = \overline{q_i} e^{ikt} \end{aligned} \tag{10}$$

where $\overline{\Delta C_P^{(F)}}$ and $\overline{q_i}$ are complex quantities.

$F_r(X, Y, T)$ of Eq. (8) can be expressed as

$$F_r(X, Y, T) = (H_r + \phi_0 Y)e^{i\omega T} - (\theta_r + b_\theta Y)(X - A)e^{i(\omega T + \phi)} \tag{11}$$

By substituting Eqs. (9–11) into Eq. (7), and by nondimensionalizing Eq. (7) using b_0, we obtain the matrix form of Eq. (7) as

$$\{[(\omega_i/\omega)^2 - 1] - [A_{ij}]\}\{\overline{q_j}\} = \{\overline{F_i}\} \tag{12}$$

where

$$A_{ij} = \frac{1}{k^2}\left(\frac{\rho b_0^4}{M_i}\right)\left\{ \int_0^s \int_{\xi_l}^{\xi_t} \overline{\Delta C_{pj}}(x, y)\phi_i(x, y)\, \mathrm{d}x\, \mathrm{d}y \right\} \tag{13}$$

$$\begin{aligned} \overline{F_i} = \frac{2b_0^3}{M_i} \int_0^s \int_{\xi_l}^{\xi_t} m(x, y)(h_r + \phi_0 y - (\theta_r + b_\theta z) \\ \times (x - a)e^{i\phi})\phi_i(x, y)\, \mathrm{d}x\, \mathrm{d}y \\ + \frac{1}{k^2}\left(\frac{\rho b_0^4}{M_i}\right) \int_0^s \int_{\xi_l}^{\xi_t} \overline{\Delta C_p^{(F)}}(x, y)\phi_i(x, y)\, \mathrm{d}x\, \mathrm{d}y \end{aligned} \tag{14}$$

$\overline{\Delta C_{pj}}$ can be computed by solving the integral equations of the lifting-surface theory [3], namely,

$$\left(ik\phi_j + \frac{\partial \phi_j}{\partial x}\right) \Big/ b_0 = \frac{1}{8\pi} \iint_S \overline{\Delta C_{pj}}(\xi, \eta) K_{WT}(x, y; \xi, \eta)\, \mathrm{d}\xi\, \mathrm{d}\eta \quad (15)$$

where K_{WT} is the kernel function. Similarly, $\overline{\Delta C_p^{(F)}}$ in Eq. (14) can be found by solving the integral equation of the lifting-surface theory [3], namely,

$$ik(h_r + \phi_0 y - (\theta_r + b_\theta y)(x - a)e^{i\phi}) - (\theta_r + b_\theta y)e^{i\phi} = \frac{1}{8\pi} \iint_S \overline{\Delta C_p^{(F)}}(\xi, \eta) K_{WT}(x, y; \xi, \eta)\, \mathrm{d}\xi\, \mathrm{d}\eta \quad (16)$$

In Eqs. (13–16), x, y, ξ, and η are dimensionless coordinates obtained by dividing the physical coordinates by b_0, a is the x coordinate of the feathering axis, h_r is the dimensionless heaving amplitude at the root station, ξ_l and ξ_t are the x coordinates of the leading and trailing edges, respectively, and s is defined by l/b_0 with l the semispan length. We employ the DLM to solve Eqs. (15) and (16).

By solving Eq. (12) for a given forced motion and the natural vibration characteristics of the wing, we can compute the load distributions $\Delta P(X, Y, T)$ using Eq. (9) in complex form as

$$\overline{\Delta P}(x, y)e^{ikt} = \frac{1}{2}\rho U^2 \overline{\Delta C_p}(x, y)e^{ikt} = \frac{1}{2}\rho U^2 \left(\overline{C_p^{(F)}}(x, y) + \sum_{j=1}^{N} \overline{\Delta C_{pj}}(x, y)\overline{q_j}\right)e^{ikt} \quad (17)$$

Once $\Delta P(x, y, t)$ is given, the time-averaged thrust and necessary power can be computed as follows. The time-averaged thrust $\bar{T}$ is composed of two components, the leading-edge suction $\overline{T_L}$ and the thrust induced by tilting the normal force vector due to the feathering motion $\overline{T_D}$:

$$\bar{T} = \overline{T_L} + \overline{T_D} \quad (18)$$

$$\bar{T} = \tfrac{1}{2}\rho U^2 S \overline{C_T} = \tfrac{1}{2}\rho U^2 S(\overline{C_{TL}} + \overline{C_{TD}}) \quad (19)$$

where $\overline{C_{TL}}$ is the thrust coefficient due to leading-edge suction and $\overline{C_{TD}}$ is the thrust coefficient due to the tilt of the normal force vector. $\overline{C_{TL}}$ can be computed by a procedure similar to that proposed by Lan [4] for the quasi-vortex lattice method.

First, we compute the leading-edge singularity parameter [4] $\overline{C_S}$ using $\overline{\Delta C_p}$ in Eq. (17):

$$\overline{C_S}(y) = \frac{1}{2}\overline{\Delta C_p}(x_{l,lp}, y)\sqrt{\frac{(x_{l,lp} - x_l)}{2}} \quad (20)$$

where $x_{l,lp}$ is the x coordinate of the midpoint of the lifting line of the leading-edge panel [3] and x_l is the x coordinate of the leading edge. It should be noted that $x_{l,lp}$ and x_l are functions of y. Using $\overline{C_S}$ thus determined, we finally compute $\overline{C_{TL}}$ as

$$\overline{C_{TL}} = \frac{2b_0^2}{S}\int_0^s \{\pi \overline{C_s^2}/(2\cos\Lambda_e)\} C(y)\, \mathrm{d}y \quad (21)$$

where $C(y)$ is the dimensionless local chord length and Λ_e is the sweep angle of the quarter chord line of the leading-edge panel. In Eq. (21), $\overline{C_S^2}$ can be given by

$$\overline{C_S^2}(y) = (C_{SR}^2(y) + C_{SI}^2(y))/2 \quad (22)$$

where C_{SR} and C_{SI} are the real and imaginary parts of $\overline{C_S}$ given by Eq. (20). It should be noted that the number of chordwise and spanwise panels should be more than 30 to obtain a converged solution of $\overline{C_{TL}}$ as clearly seen in Fig. 3.

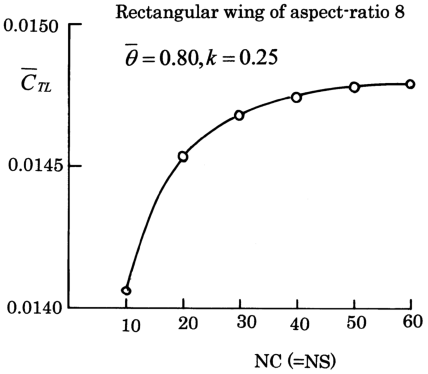

Fig. 3 Convergence history of $\overline{C_{TL}}$ for a rectangular wing oscillating in a coupled heaving and pitching oscillation.

$\overline{C_{TD}}$ can be given by

$$\overline{C_{TD}} = \overline{T_D} \Big/ \left(\frac{1}{2}\rho U^2 S\right) = \frac{1}{T^*}\int_0^{T^*} \left\{ \iint_S \mathrm{Re}(\overline{\Delta P}(X, Y)e^{i\omega T}\mathrm{Re} \times \left(\frac{\partial F}{\partial X}\right) \mathrm{d}X\, \mathrm{d}Y \right\} \mathrm{d}T \Big/ \left(\frac{1}{2}\rho U^2 S\right) \quad (23)$$

where Re indicates the real part of a complex quantity and T^* is the period of the forced oscillation. We can easily derive the working form of $\overline{C_{TD}}$ by substituting Eq. (17) and the complex form of Eq. (1) into Eq. (23). The time mean necessary power coefficient $\overline{C_{PW}}$ can be given by

$$\overline{C_{PW}} = \bar{W} \Big/ \left(\frac{1}{2}\rho U^3 S\right) = -\frac{1}{T^*}\int_0^{T^*} \left\{ \iint_S \mathrm{Re}(\overline{\Delta p}(X, Y)e^{i\omega T})\mathrm{Re} \times \left(\frac{\partial F}{\partial T}\right) \mathrm{d}X\, \mathrm{d}Y \right\} \mathrm{d}T \Big/ \left(\frac{1}{2}\rho U^3 S\right) \quad (24)$$

where $\bar{W}$ is the time mean rate of work. We can easily derive the working form of $\overline{C_{PW}}$ by substituting Eq. (17) and the complex form of Eq. (1) into Eq. (24). Then the propulsive efficiency η_p is defined by

$$\eta_p = \frac{\bar{T}U}{\bar{W}} = \frac{\overline{C_T}}{\overline{C_{PW}}} \quad (25)$$

To evaluate the accuracy of the present DLM code modified to take into account the leading-edge suction force, the η_P and $\overline{C_T}$ for an oscillating rectangular wing of aspect ratio 8 are computed. For this case, the results obtained by Chopra and Kambe [5] and those of Lan [4] are available. These three methods are compared to each other in Figs. 4a and 4b. For this case, the whole wing conducts the pure heaving oscillation or a coupled heaving and pitching oscillation. In the figures, $\bar{\theta}$ is the feathering parameter defined by

$$\bar{\theta} = \theta_r U/(H_r\omega) \quad (26)$$

$\bar{\theta} = 0$ corresponds with the pure heaving oscillation, and $\bar{\theta} = 0.8$ corresponds with the coupled heaving ($H_r = 2b_0$) and pitching oscillation with the amplitude of $\theta_r = \bar{\theta}k(H_r/b_0)$ with $a = 0.5$ and $\phi = 90$ deg. It should be noted that the thrust is generated entirely from the leading-edge suction force for $\bar{\theta} = 0$. As to η_p, the agreement of the present computation with those of Lan [4] and Chopra and Kambe [5] are good except for $\bar{\theta} = 0.8$ in $k = 0.8$–1.0, where the agreement is not as good. As to C_T, the results of the present computation show close agreement with those of Chopra and Kambe [5] both for $\bar{\theta} = 0$ and $\bar{\theta} = 0.8$, while some discrepancy is observed for those of Lan [4], especially for $\bar{\theta} = 0$. The reasons for these discrepancies are not known because no exact solution is available for comparison.

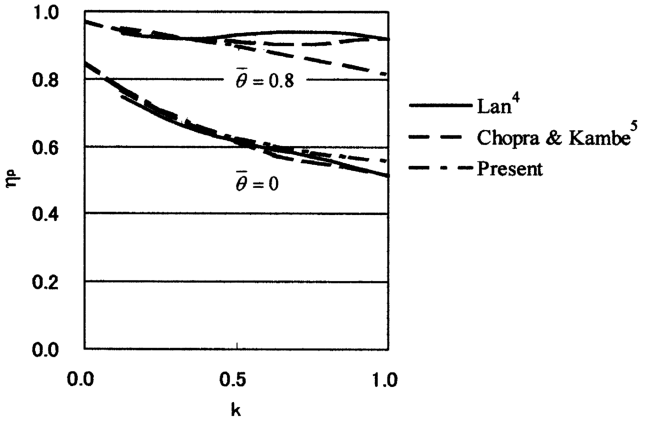

a) Propulsive efficiency

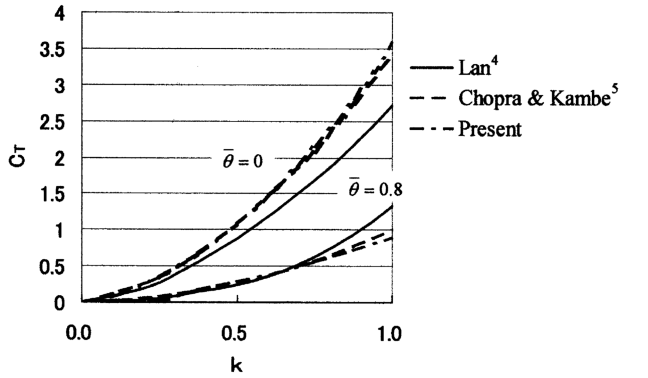

b) Thrust coefficient

Fig. 4 Comparison with other methods for a rectangular wing of aspect ratio 8 in pitching about a 3/4 chord line and in heaving.

III. Evaluation of Aeroelastic Response Computation Capability by Comparison with Other Methods and Experiments

To evaluate the accuracy and reliability of the present procedure for computing the aeroelastic response of a flapping wing, we have applied the present method to the flapping wing studied by DeLaurier in [2]. In Fig. 5, the planform of the flapping wing studied by DeLaurier is shown. The semispan and the root chord lengths are 43 and 11 in., respectively. The full span aspect ratio is 9.4. All the structural parameters such as the elastic axis location, the elastic properties (EI, GJ distributions) and inertial properties which are necessary to apply the present method are provided in [2]. The theoretical results obtained by using Combo Wing and the experimental data which are obtained for the condition of $\alpha_m = 6$ deg and $U = 45$ ft/s in the wind tunnel are also reported in [2]. In Figs. 6a and 6b, the theoretical and experimental results of time-averaged thrust and lift are shown with respect to the frequency of the forced oscillation. Note that the thrust and lift shown in Fig. 6 are for the semispan wing.

In the present computations of the time-averaged thrust, the time mean induced drag due to the time mean lift and the viscous drag ($C_{df} = 0.0120$ used in [2] is assumed) are also taken into account. As seen in Fig. 6a, the present method predicts about 0.10 lbf higher values than those of the experiment and the strip theory of [2], though the results of the present method show almost the same trend as those of the experiment and the strip theory of [2]. The reason for this discrepancy might be attributed to the effects of flow separation observed in the wind-tunnel experiment [2].

As to the average lift shown in Fig. 6b, the results of the present method using the lifting-surface theory including the aeroelastic effect show about 20% lower values than those of the experimental results of [2]. One of the reasons for this discrepancy might be

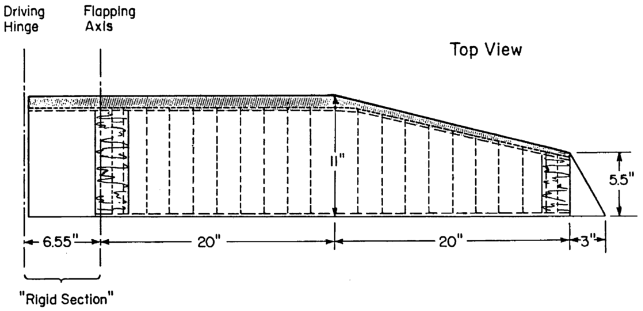

Fig. 5 Wing planform [2].

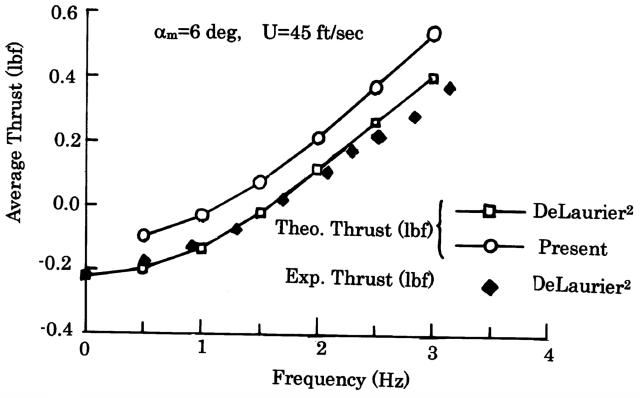

a) Average thrust

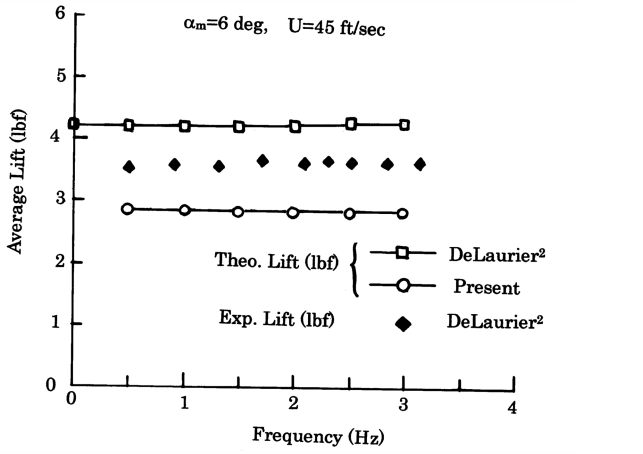

b) Average lift

Fig. 6 Wing performance.

attributed to the fact that the airfoil camber is not taken into account in the present computation.

In Figs. 7a and 7b, the spanwise dynamic response distributions, namely, the feathering and flapping amplitudes ($\overline{\theta_e}$ and $\overline{H_e}$) and their phase angles ($\phi_{\theta e}$ and ϕ_{he}) are compared to those predicted by DeLaurier [2] using Combo Wing and the present method. As to $\overline{\theta_e}$, the present procedure predicts almost the same value as that predicted by DeLaurier at the tip station although the present method predicts a smaller feathering amplitude than those predicted by DeLaurier for other spanwise stations. As to $\overline{H_e}$, the agreement between the two methods is good from the root to the tip stations. As to the agreement between the two methods for the distributions of $\phi_{\theta e}$ and ϕ_{he}, about 10 deg of differences are observed between the two. Note that the experimental data for these dynamic response distributions are not available.

η_p and $\overline{C_T}$ for the zero lift condition, which are predicted by the present method, are 72% and 0.099, respectively. Therefore, DeLaurier's design of this wing is quite efficient though the

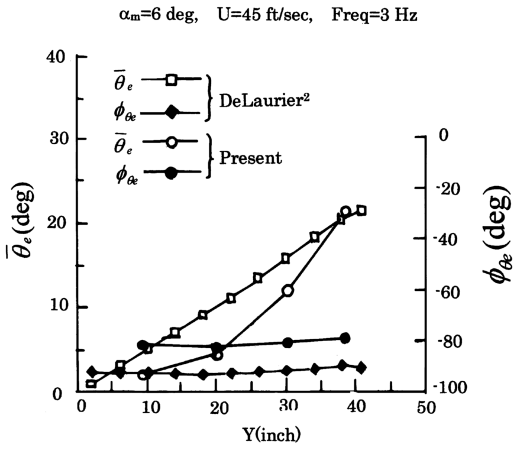

a) Feathering amplitude and phase angle

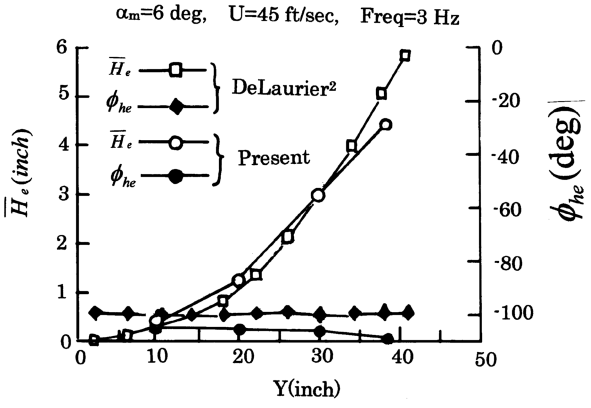

b) Flapping amplitude (due to aeroelastic effect) and phase angle

Fig. 7 Dynamic response distributions.

optimization was conducted by trial and error. (The results of the optimum flapping wing design for this wing by using the present automated design procedure will be given in a later section.)

As for the conclusion of this section, it can be said that the present method of computing the aeroelastic response of a flapping wing by using DLM is reliable.

IV. Optimum Aeroelastic Design Using the Complex Method

By combining the general method for computing the aeroelastic effects of an elastic flapping wing, described in the previous section, and an optimization algorithm, we can conduct an optimum structural design of a flapping wing. For the optimization algorithm, we employed the complex method, originally proposed by Box [6]. The complex method is a direct search method that can handle multiple constraints without recourse to gradients. In the present study, we applied the optimization procedure to the design of a birdlike UAV that flies slowly like a Kite Hawk (*Milvus migrans*). As is well known, the Kite Hawk is an expert of an efficient flight, namely, it finds the thermal convection and can perform continuous flight only by occasional flapping. If we could develop an UAV that imitates such flight of the Kite Hawk, it might provide a highly efficient (long duration) UAV. In Fig. 8, the planform and structural arrangement of the semispan wing of the Kite Hawk UAV are shown. The full span of the wing is 1.68 m and the root chord length is 0.28 m. The full span aspect ratio and wing area are 6 and 0.471 m^2, respectively. The total mass of the UAV is assumed to be about 300 g. The wing can sustain a total weight of 2.94 N at a cruising speed of 4.13 m/s at $C_L = 0.598$. The structural component consists of only a straight main spar that can bend and twist and which is located near the leading edge, as shown in Fig. 8. The ribs are

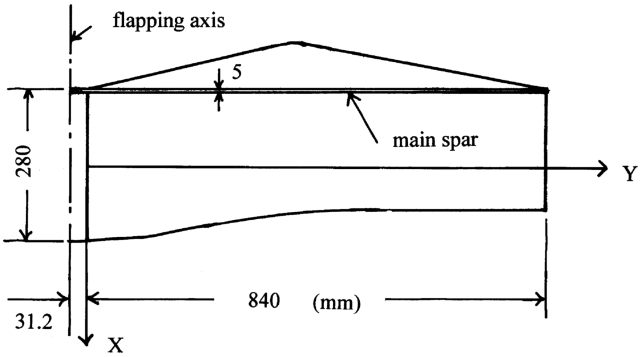

Fig. 8 Planform of the Kite Hawk (*Milvus migrans*) UAV.

assumed to be firmly attached to the main spar and are chordwise rigid. It is assumed that the flapping wing motion is caused only by the dihedral flapping motion of the main spar. Therefore, the feathering motion is induced only by the aeroelastic response.

The purpose of the optimization study is to determine the thickness distribution of the main spar that generates the ideal bending and twisting motions to attain maximum propulsive efficiency. This section of the main spar is assumed to be rectangular and its width is assumed to be a constant 5 mm in the spanwise direction. The thickness distribution is assumed to be a parabolic function of y. We select thicknesses t_1, t_2, and t_3 at the root, mid-semispan, and tip stations, respectively, as design variables to determine the structural characteristics. In addition to these design variables, we select k, ϕ_0, and a as design variables that determine the flapping wing motion. Therefore, there are six design variables in total. The objective function is the propulsive efficiency η_p. The following constraints are imposed, $\overline{C_T} \geq C_D$ and $t_1 \geq t_2 \geq t_3$, where C_D is the total drag coefficient of the UAV. Because the flapping wing is composed of a single spar, we employ a simple beam theory [7] to compute the natural vibration modes. The distributions of the mass m, static unbalance S_y, and the moment of inertia I around the main spar are taken to be the concentrated quantities at the center of the segment obtained by dividing the main spar into 13 equally spaced portions. It should be noted that the inertial data of the main spar itself change at each iteration step of the optimization process. The value of the concentrated mass, imbalance, and inertia at each segment are assumed to be equal and given as $m_i = 0.005$ kg, $Sy_i = 7.0 \times 10^{-5}$ kgm, and $I_i = 5.0 \times 10^{-5}$ kgm^2, for $i = 1$–13. The main spar is assumed to be a quasi-isotropic laminate construction of carbon fiber reinforced plastic (CFRP) with elastic properties $E_L = 181$ Gpa, $E_T = 10.3$ GPa, $G_{LT} = 7.17$ GPa, and $\nu = 0.28$.

The optimization process proceeds by the use of flexible figures of $K > N + 1$ vertices in N dimensional design space, where N is the number of design variables, $N = 6$ in the present problem, and we

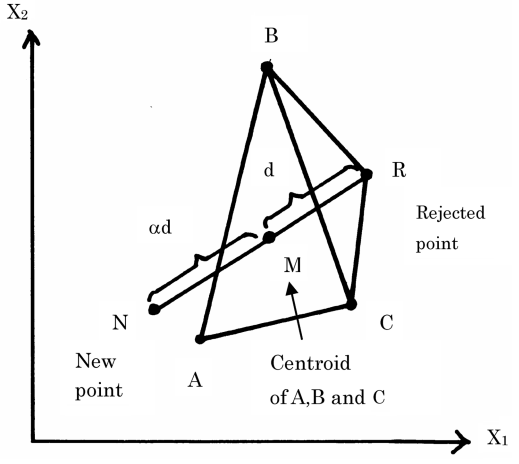

Fig. 9 Complex method.

Table 1 Results of intermediate iterative steps

Iteration step	η_p	$\overline{C_T}$	$\overline{C_{pW}}$	k	ϕ, deg	a	t_1, mm	t_2, mm	t_3, mm
Baseline	0.670	0.267	0.398	0.300	40	−0.50	7.00	2.00	1.00
10	0.685	0.177	0.254	0.251	44	−0.78	7.31	1.82	0.77
20	0.733	0.188	0.257	0.233	46	−0.94	6.68	1.98	0.91
30	0.741	0.155	0.209	0.219	45	−0.85	6.49	1.98	0.83
40	0.748	0.163	0.218	0.214	47	−0.91	6.09	2.08	0.88
50	0.754	0.166	0.220	0.213	49	−0.99	5.76	2.08	0.92

Table 2 Comparison of the original design and the optimum design

	η_p	k	U, m/s	ϕ_0, deg	$\overline{C_T}$	$\overline{C_W}$
Original design	0.715	0.192	13.72	27.3	0.099	0.139
Optimum design	0.754	0.164	16.0	40.9	0.104	0.137

have taken $K = 9$ vertices. In Fig. 9, four vertices (the points A, B, C, and R) are shown for illustration purposes. Each vertex corresponds to a specific wing motion specified by the six design variables in the present problem. The objective function (the propulsive efficiency η_p) and the constraint function $\overline{C_T}$ at each vertex are evaluated using the method described in the previous section. Then, the worst vertex (the vertex that gives the lowest propulsive efficiency, point R in Fig. 9) is found, and is rejected. A new point N is found such that the new point is located at a distance αd from the centroid M of the vertices A, B, and C in the opposite direction to R, where d is the distance between M and R, and where α is a coefficient used to accelerate the convergence, usually taken as $\alpha = 1.0$–1.3. We call this process rule 1.

Next the objective function η_p and the constraint function $\overline{C_T}$ at the new point N are evaluated using the method described in the previous section. If the constraint function does not satisfy the specified value of the constraint, namely, $\overline{C_T} < C_D$, the point N is shifted toward the centroid M such that the distance between the new point N and M is half the previous distance. We call this process rule 2. Rule 2 is repeated until the constraint is satisfied.

Rule 1 and rule 2 are repeated until the converged value of η_p is obtained. The six design variables that give a maximum η_p give the optimum flapping wing motion and the optimum thickness distribution of the main spar. Further details of the complex method are explained in [8]. In the present problem we set C_D to be 0.15. This value is considerably higher than the value of 0.055 estimated by the

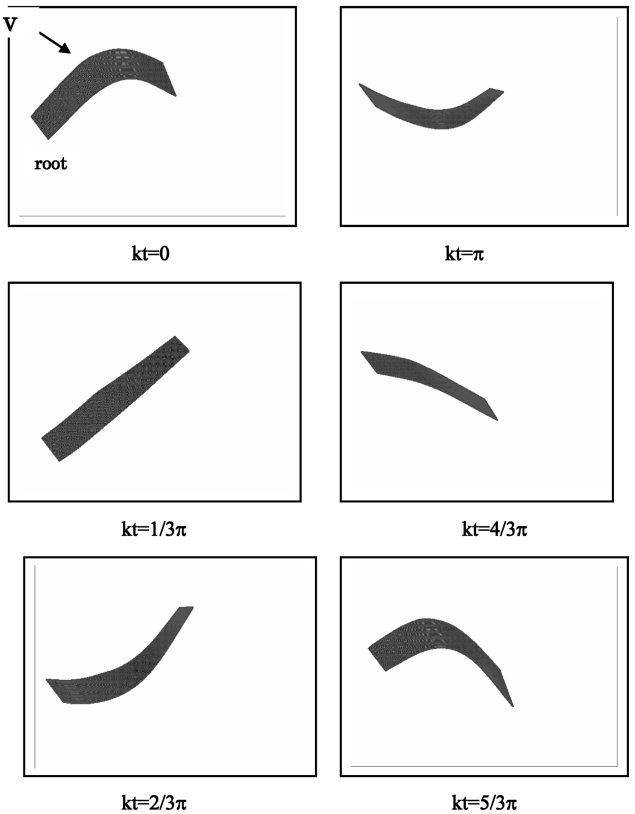

Fig. 10 Wing deformation during one cycle of oscillation.

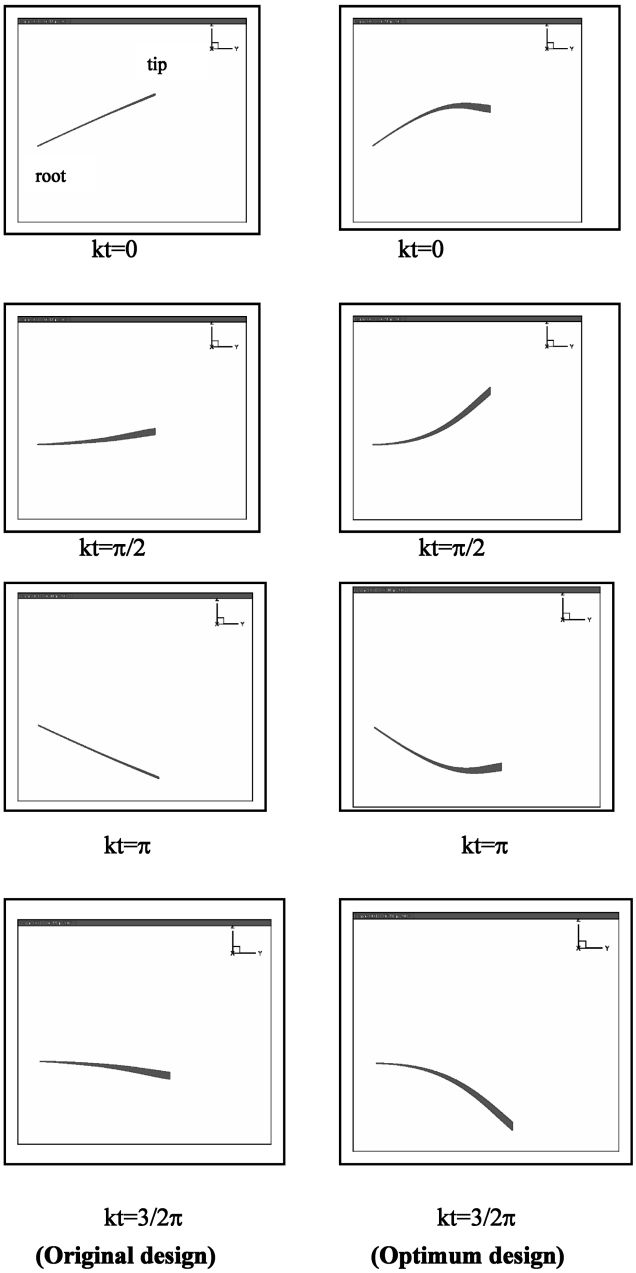

Fig. 11 Wing deformations of original and optimum designs (back view).

DLM code (assuming a minimum drag coefficient of 0.04 and an induced drag coefficient of 0.015 at $C_L = 0.598$). However, we assumed the DLM code would underestimate C_D as it does not account for viscous effects. This choice of $C_D = 0.15$ will be justified in the next section by the numerical simulation using a Navier–Stokes code.

A. Results of Optimization Using DLM

A converged solution was obtained after 50 iterations. The results were as follows: $\eta_p = 0.754$, $\overline{C_T} = 0.166$ ($\overline{C_{TL}} = 0.089$, $\overline{C_{TD}} = 0.077$), $\overline{C_{PW}} = 0.220$, $k = 0.213$, $\phi_0 = 48.9$ deg, $a = -0.986$, $t_1 = 5.76$ mm, $t_2 = 2.08$ mm, and $t_3 = 0.92$ mm.

In Table 1, the results of the intermediate iterative steps are also shown. As seen in the table, the propulsive efficiency is improved about 13% over the baseline configuration. It should be noted that the propulsive efficiency of the baseline configuration is 67% which seems to be already efficient.

The propulsive efficiency of 75% seems quite high. (Note that 75% of η_p is obtained for a mean angle of attack of 0 deg. Therefore, the induced drag due to the averaged lift is not taken into account in evaluating η_p.) Because the optimum value of the reduced frequency is 0.213, we can easily determine the cruising velocity to be $U_C = 4.13$ m/s by assuming a forced flapping frequency of 1 Hz. We can then easily estimate $C_L = 0.598$ to sustain a weight of 2.94 N at $U_C = 4.13$ m/s. The time mean necessary power $\bar{W}$ is 4.47 W and the power-mass ratio for this UAV is 14.9 W/kg, which seems quite efficient. The natural frequencies of the wing are $f_1 = 1.65$ Hz (first bending predominant), $f_2 = 5.93$ Hz (first torsion predominant), $f_3 = 13.7$ Hz (second torsion predominant). The six total natural vibration modes are employed in computing the aeroelastic responses. In Fig. 10, the wing deformations during one cycle of oscillation are shown. (Note that the wing displacement shown in Fig. 10 is not exaggerated.) As can be seen, the wing is very flexible and bends in the spanwise direction and twists around the main spar. From animations of the wing deformation sequence we can confirm that a spanwise traveling wave is generated.

B. Optimum Design of DeLaurier's Ornithopter Wing

It seems interesting to apply the present optimization procedure to DeLaurier's ornithopter wing [2] discussed in the previous section and to see the difference between the original design and the present optimum design. For the present optimization study, we employ the same wing structure as that of our Kite Hawk UAV; that is, the stiffness and the strength member of the wing is only the main spar. The width of the main spar is assumed to be 0.01 m, and its spanwise thickness distribution is determined by the optimization to maximize the propulsive efficiency. The material of the main spar is the same CFRP as used in our Kite Hawk UAV design. The same inertial properties as those of the DeLaurier's ornithopter wing are used. The flapping frequency is assumed to be 3 Hz of the original design and C_D is assumed to be 0.10 because the $\overline{C_T}$ of the original wing at zero lift condition, which is computed by our DLM cod, is 0.099. We have obtained the converged solution after 50 iterations. The results of the optimum design are compared with those of the original wing in Table 2.

The thickness of the main spar, namely, t_1, t_2, and t_3 are determined as 12.7, 5.26, and 1.93 mm, respectively. The zero lift propulsive efficiency of the optimum design is about 5% higher than that of the original wing. Although the propulsive efficiencies of both designs show little difference, some appreciable differences are observed in the cruise velocity and flapping amplitude. In Fig. 11, the wing deformations of both designs are compared. As seen in the figure, the present optimum design is highly flexible in the spanwise

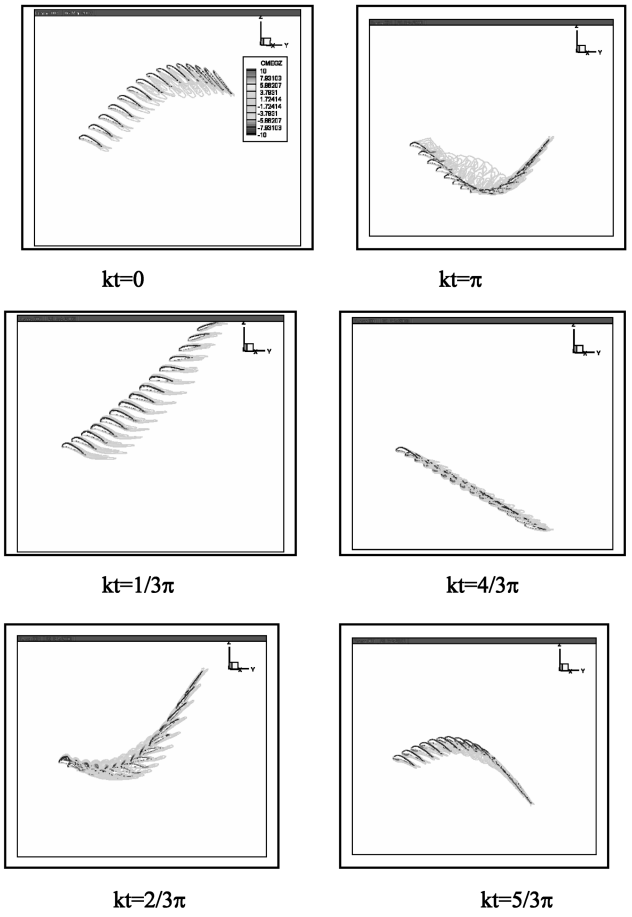

Fig. 12 Wing deformation and flow patterns (ω_y) during one cycle of oscillation.

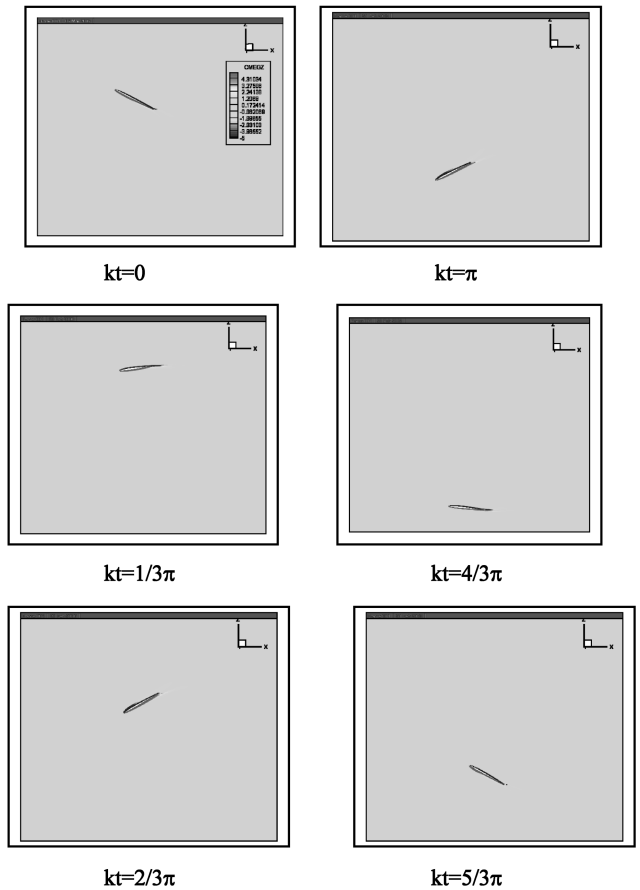

Fig. 13 Flow pattern (ω_y) at a 91% semispan station.

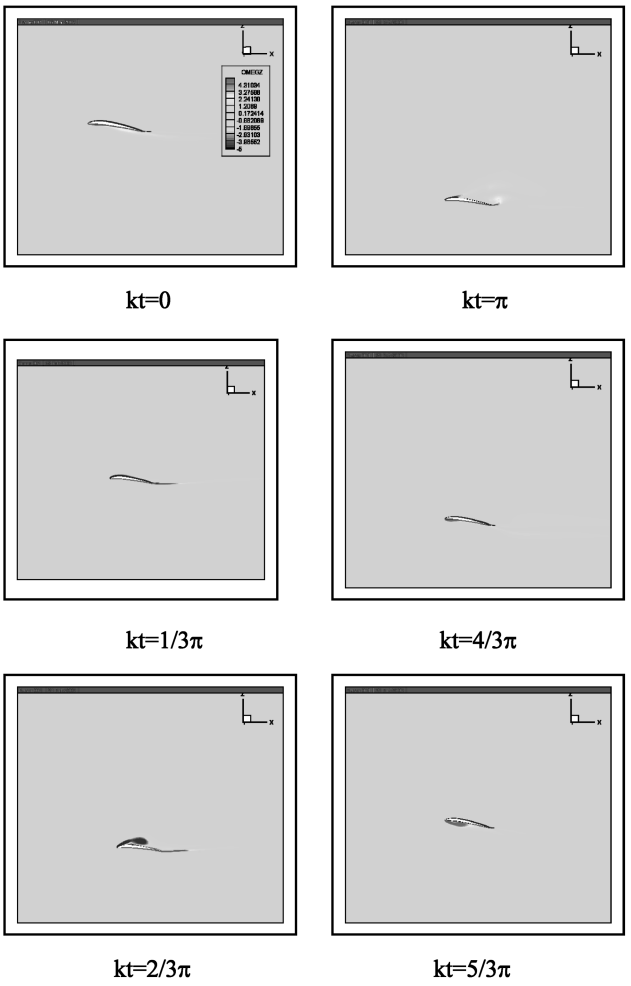

Fig. 14 Flow pattern (ω_y) at a 30% semispan station.

direction while the original design is quite rigid in the spanwise direction.

V. Numerical Simulation of Kite Hawk UAV Using Navier–Stokes Code

To evaluate the viscous effect on the optimum design of the Kite Hawk UAV, which is obtained using DLM as the aerodynamic tool, a numerical simulation was conducted using the three-dimensional NS code developed by Isogai [9]. Equation (7) was incorporated into the NS code and the aeroelastic response of the wing was computed by solving Eq. (7) at each time step using the wing boundary condition (computed from the wing deformation obtained at one time step before). The natural vibration modes obtained for the optimum aeroelastic design described in the previous section were used for the aeroelastic response computation using the NS code. A C–H-type structural grid system was used with 240 grid points in the chordwise direction, 23 spanwise and 51 in the direction normal to the wing surfaces. The wing sections employed in the present NS simulation were generated by modifying the NACA0012 airfoil section by changing the thickness ratio, introducing camber, and setting the maximum camber location. The amount of camber for local airfoil sections was changed parabolically from the root to the tip stations so that the camber at the root was maximum and that at the tip was zero. The thickness ratio of the present section was 6% and the maximum camber was 6% of the chord located 30% from the leading edge. The mean angle of attack was set as 8 deg. The Reynolds number based on the root chord was 7.63×10^4 and the Baldwin and Lomax algebraic turbulence model [10] was employed.

The results obtained are as follows: $\overline{C_T} = 0.046$, $\overline{C_L} = 0.552$, and $\overline{C_{PW}} = 0.242$.

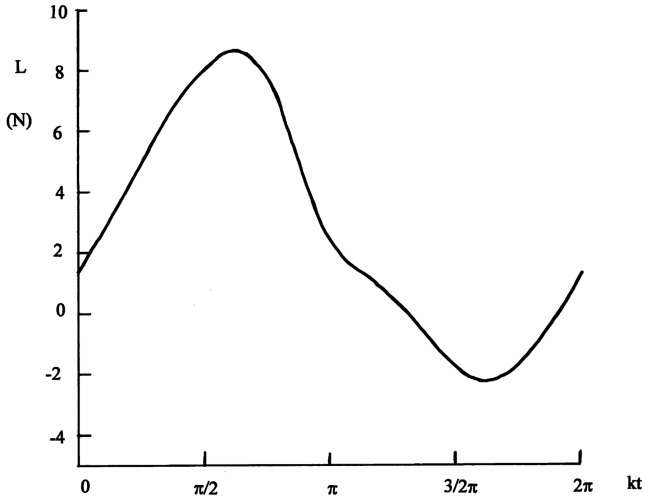

Fig. 15 Variation of lift during one cycle of oscillation. ($\bar{L} = 2.71$ N).

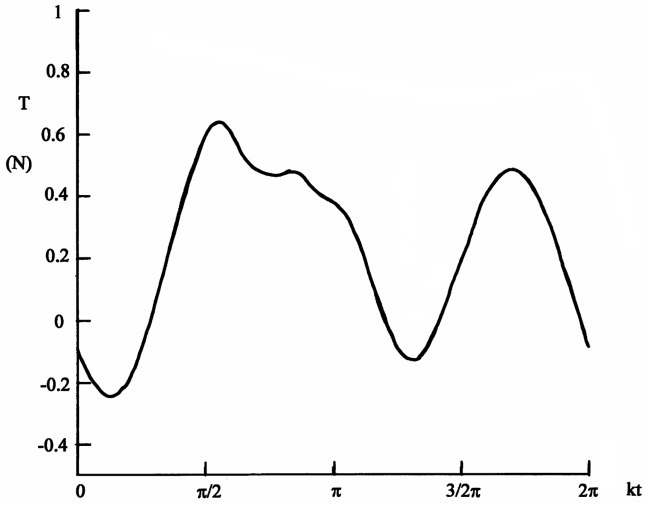

Fig. 16 Variation of thrust during one cycle of oscillation. ($\bar{T} = 0.227$ N).

These coefficients give the following physical values at $U_C = 4.13$ m/s: $\bar{T} = 0.227$ N, $\bar{L} = 2.71$ N, and $\bar{W} = 4.91$ W.

Based on these results, the wing can sustain a drag of 0.227 N and a weight of 2.71 N with a time mean power of 4.91 W and a power-mass ratio of 17.7 W/kg. These results show that the optimum aeroelastic design using DLM is still good even when viscous effects are taken into account. In Fig. 12, the wing deformations and flow patterns (isovorticity ω_y) during one cycle of oscillation are shown. To see the flow patterns in detail, the isovorticity distributions around the airfoil sections at 91 and 30% semispan stations are also shown in Figs. 13 and 14, respectively. As seen in Fig. 13, no flow separation is observed at the 91% semispan station, which attains efficient thrust generation. However, as shown in Fig. 14, large-scale flow separation can be seen at the 30% semispan station, which seems to generate the drag. The flow separation observed in the inboard portion of the wing might be the main cause of the reduction of $\overline{C_T}$ compared with that predicted by DLM. In Figs. 15–17, the time histories of lift, thrust, and rate of work during one cycle of oscillation are shown, respectively.

VI. Conclusions

A general method for the optimum aeroelastic design of a flapping wing employing a lifting-surface theory as an aerodynamic tool and the complex method as the optimization algorithm is presented. First, the capability of the present method for computing the aeroelastic

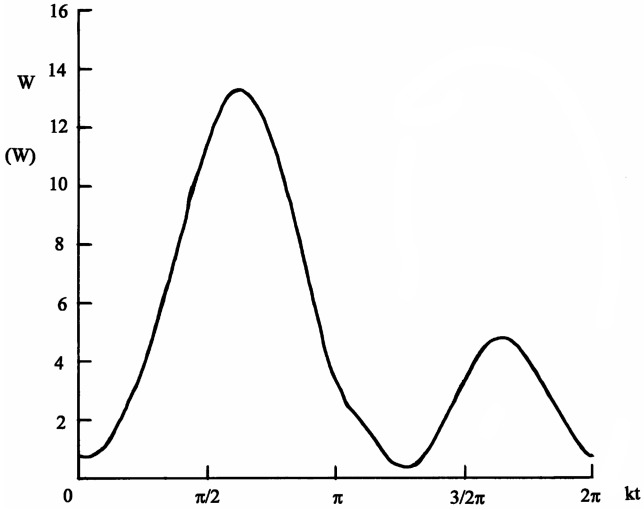

Fig. 17 Variation of rate of work during one cycle of oscillation. ($\bar{W} = 4.9$ W).

response of the flapping wing is evaluated by applying the method to DeLaurier's ornithopter wing, for which the theoretical and experimental results are available. Fairly good agreement between the present and those of DeLaurier is obtained, though some discrepancy is observed which might be attributed to the viscous effects such as flow separation. Then, the present optimum design method is applied to the Kite Hawk UAV and the optimum thickness distribution of the main spar is determined. As a result of optimization, a high propulsive efficiency of 75% is attained considering only dihedral flapping of the main spar. To evaluate the viscous effect on this optimum design using DLM, the numerical simulation using the Navier–Stokes code is conducted. It is found that the flow separation is suppressed around the outboard portion of the wing that enables the efficient thrust generation, while the large-scale flow separation is observed around the inboard portion that degrades the propulsive efficiency. Although some degradation of the propulsive efficiency due to a viscous effect is expected, it is believed that the present optimum design method using DLM might provide a useful aeroelastic design tool for a flapping wing of UAV.

References

[1] DeLaurier, J. D., and Harris, J. M., "A Study of Mechanical Flapping-Wing Flight," *Aeronautical Journal*, Oct. 1993, pp. 277–286.

[2] DeLaurier, J. D., "The Development of an Efficient Ornithopter Wing,'' *Aeronautical Journal*, May 1993, pp. 153–162.

[3] Albano, E., and Rodden, W. P., "Doublet-Lattice Method for Calculating Lift Distributions on Oscillating Surfaces in Subsonic Flows," *AIAA Journal*, Vol. 7, Feb. 1969, pp. 279–285.

[4] Lan, C. E., "The Unsteady Quasi-Vortex-Lattice Method with Applications to Animal Propulsion," *Journal of Fluid Mechanics*, Vol. 93, No. 4, 1979, pp. 747–765. doi:10.1017/S0022112079002019

[5] Chopra, M. G., and Kambe, T., "Hydromechanics of Lunate-Tail Swimming Propulsion. Part 2," *Journal of Fluid Mechanics*, Vol. 79, No. 1, 1977, pp. 49–69. doi:10.1017/S0022112077000032

[6] Box, M. J., "A New Method of Constrained Optimization and a Comparison with Other Methods," *Computer Journal*, Vol. 8, 1965, pp. 42–52.

[7] Bisplinghoff, R. L., Ashley, H., and Halfman, R. L., *Aeroelasticity*, Addison Wesley, Reading, MA, 1955.

[8] Beveridge, G. S. G., and Schecheter, R. S., *Optimization*, Theory and Practice, Chemical Engineering Series, McGraw–Hill, New York, 1970, pp. 453–456.

[9] Isogai, K., "Numerical Simulation of Unsteady Viscous Flow Around a Flapping Wing," *Computational Fluid Dynamics 2002, Proceedings of the Second International Conference on Computational Fluid Dynamics*, ICCFD, Sydney, Australia, July 2002, pp. 701–706.

[10] Baldwin, B. S., and Lomax, H., "Thin Layer Approximation and Algebraic Model for Separated Turbulent Flows," AIAA Paper 78-257, Jan. 1978.